Supplement of

Mixing state of Carbonaceous Aerosol Emissions from an Ecodesign Woodstove

Zixuan Cheng et al.

Correspondence to: James Allan (James.Allan@manchester.ac.uk)

Text S1 DMS500 default calibration was set as diesel calibration which allows inversion the ring current (Figure S1 d, e, f) in two modes which are nucleation mode (< 35 nm, spherical) and accumulation mode (> 35 nm, agglomerate). However, the size range and morphology for wood combustion aerosols are different from diesel exhaust aerosols. Applying diesel calibration to wood combustion data overestimates accumulation mode particle number (Figure S1 b) and introduces a fake peak at 50 nm in flaming phase (Figure S1 h).

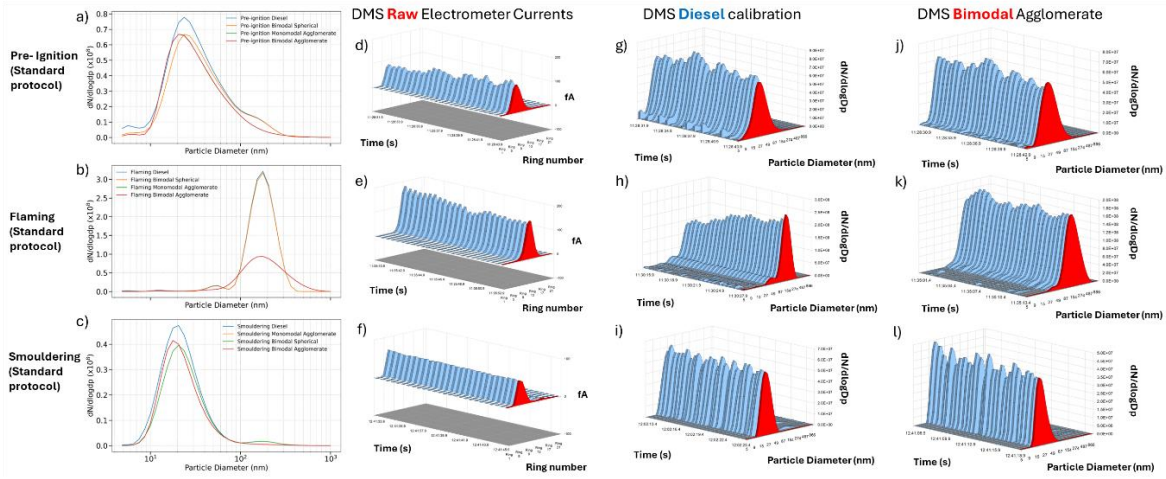

Figure S1 Pre-ignition (a), flaming (b) and smouldering (c) phases particle size distribution measured by DMS500 under raw data (d, e, f), diesel calibration (g, h, i), and bimodal agglomerate (j, k, l)

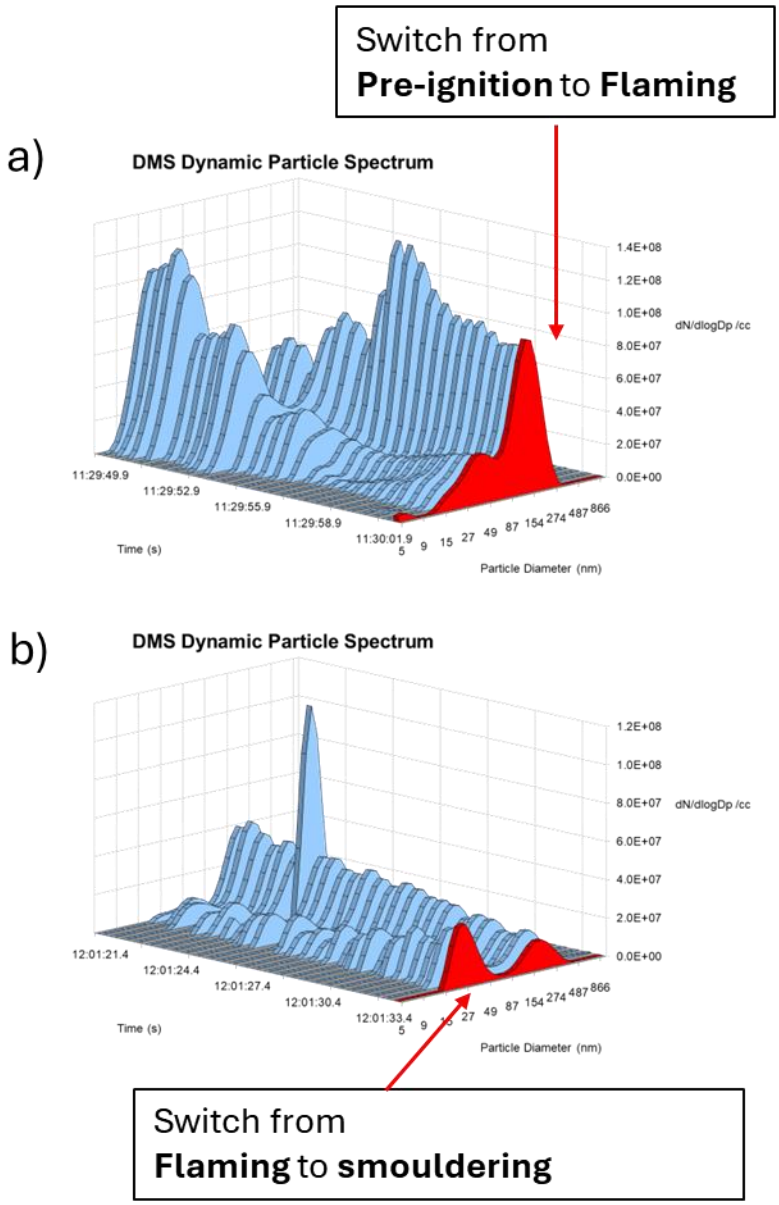

Figure S2 Definition of transition between pre-ignition and flaming (a) and flaming to smouldering (b).

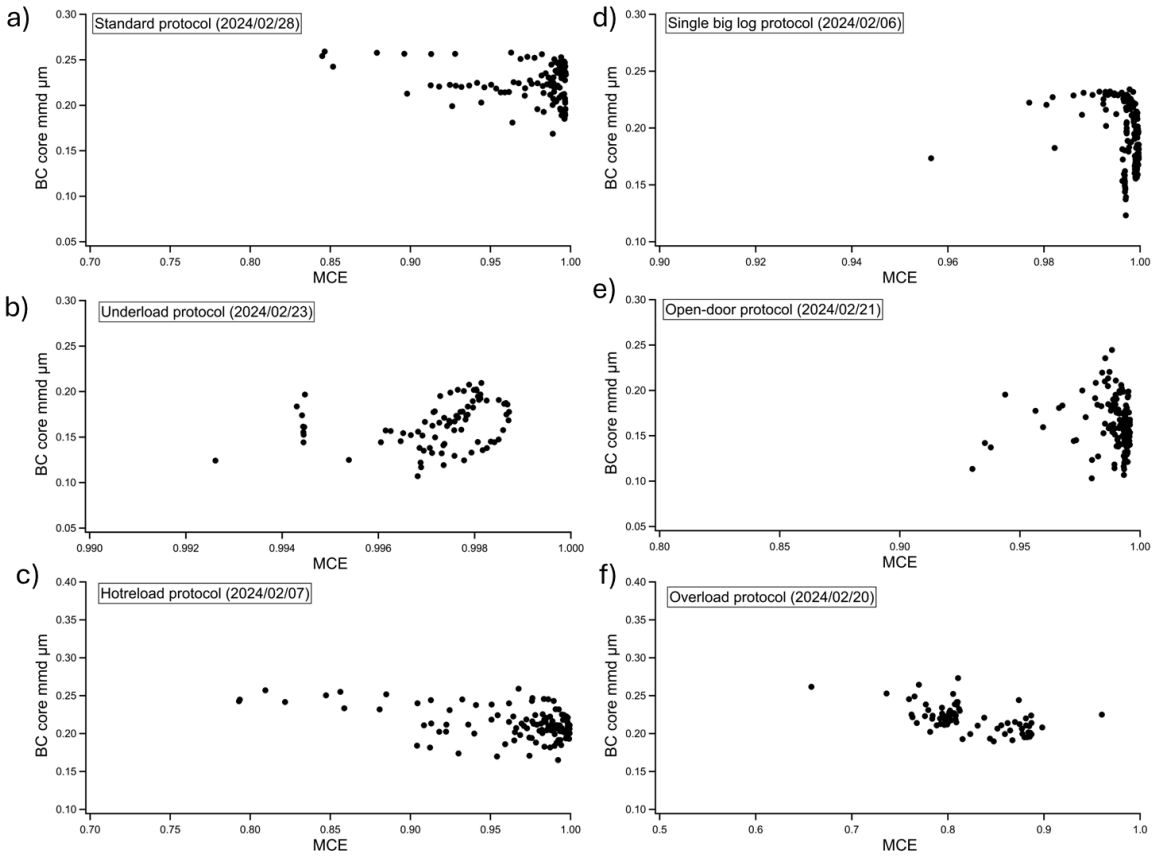

Figure S3 Scatter plots of the correlation between BC core mmd and MCE.

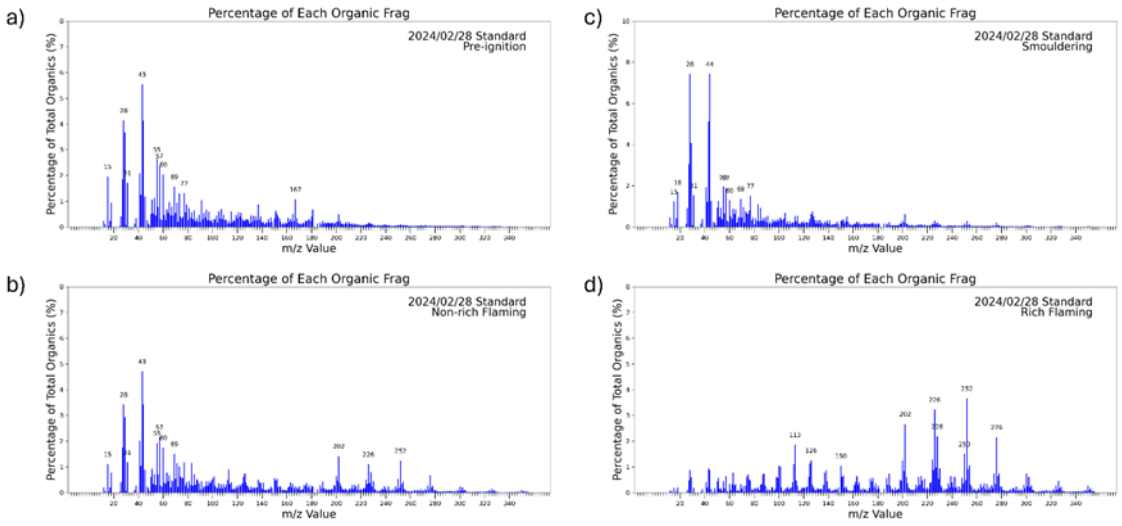

Figure S4 Averaged mass spectra of Organic Aerosols as a percentage of total OM from AMS, during a) pre-ignition, b) non-rich flaming, c) smouldering, and d) rich flaming for standard protocol.

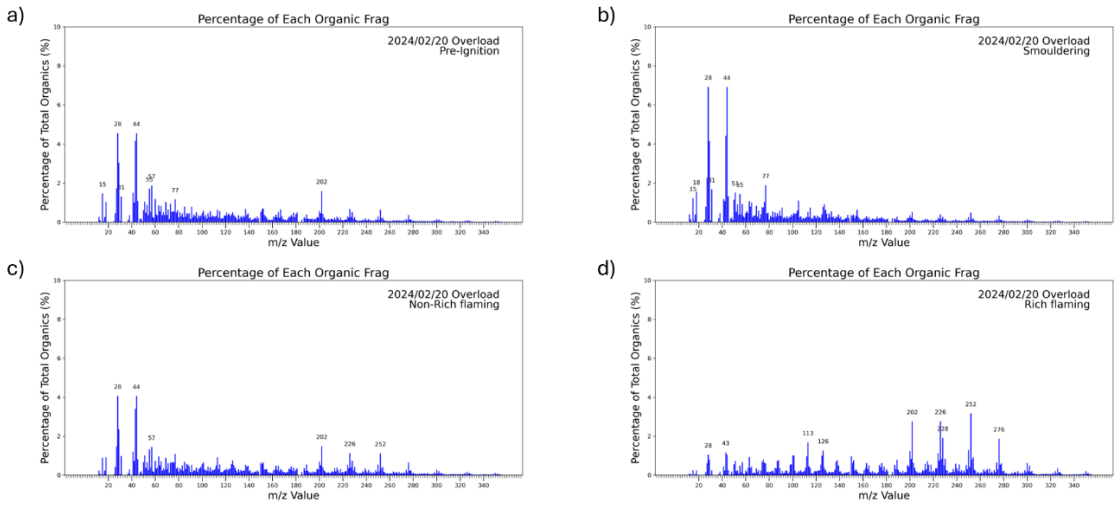

Figure S5 Mass spectra from AMS for Overload protocols by phases.

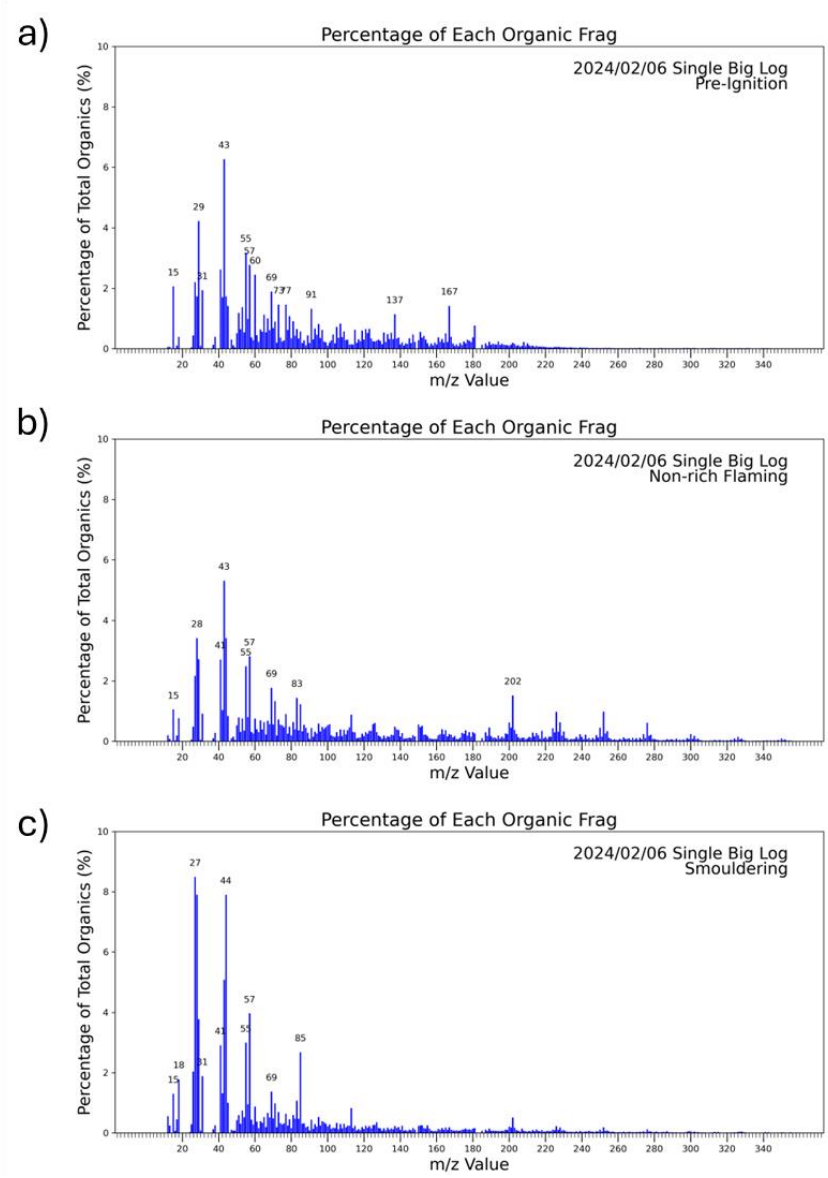

Figure S6 Mass spectra from AMS for single big log protocols by phases.

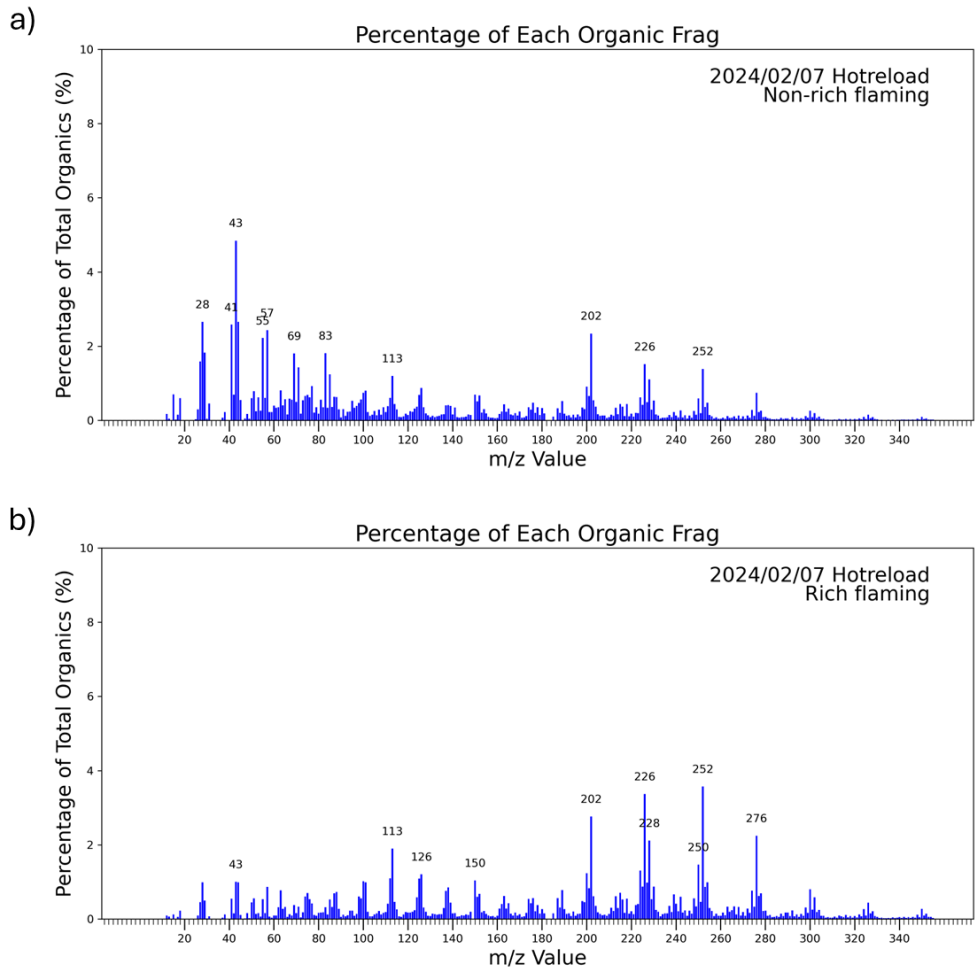

Figure S7 Mass spectra from AMS for hot reload protocols by phases.

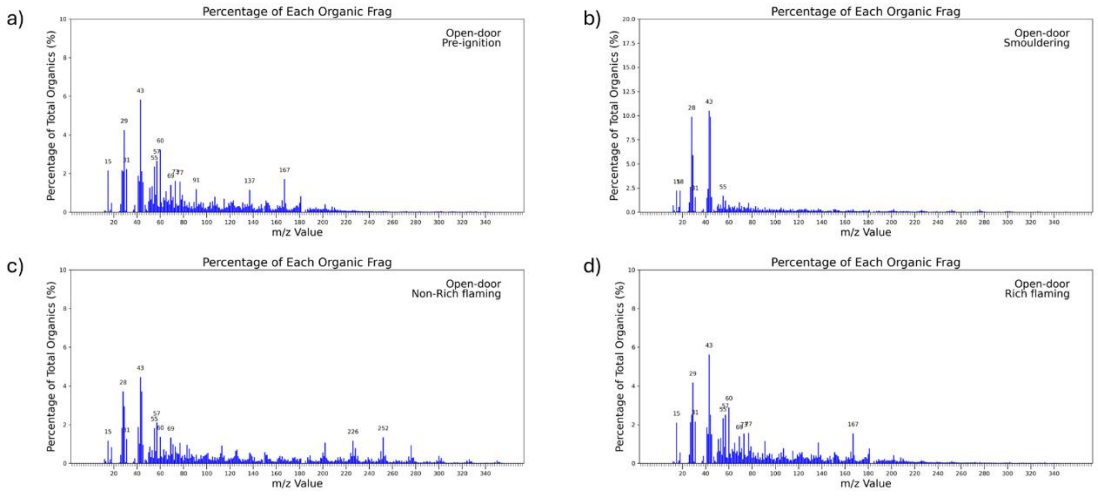

Figure S8 Mass spectra from AMS for open-door protocols by phases.

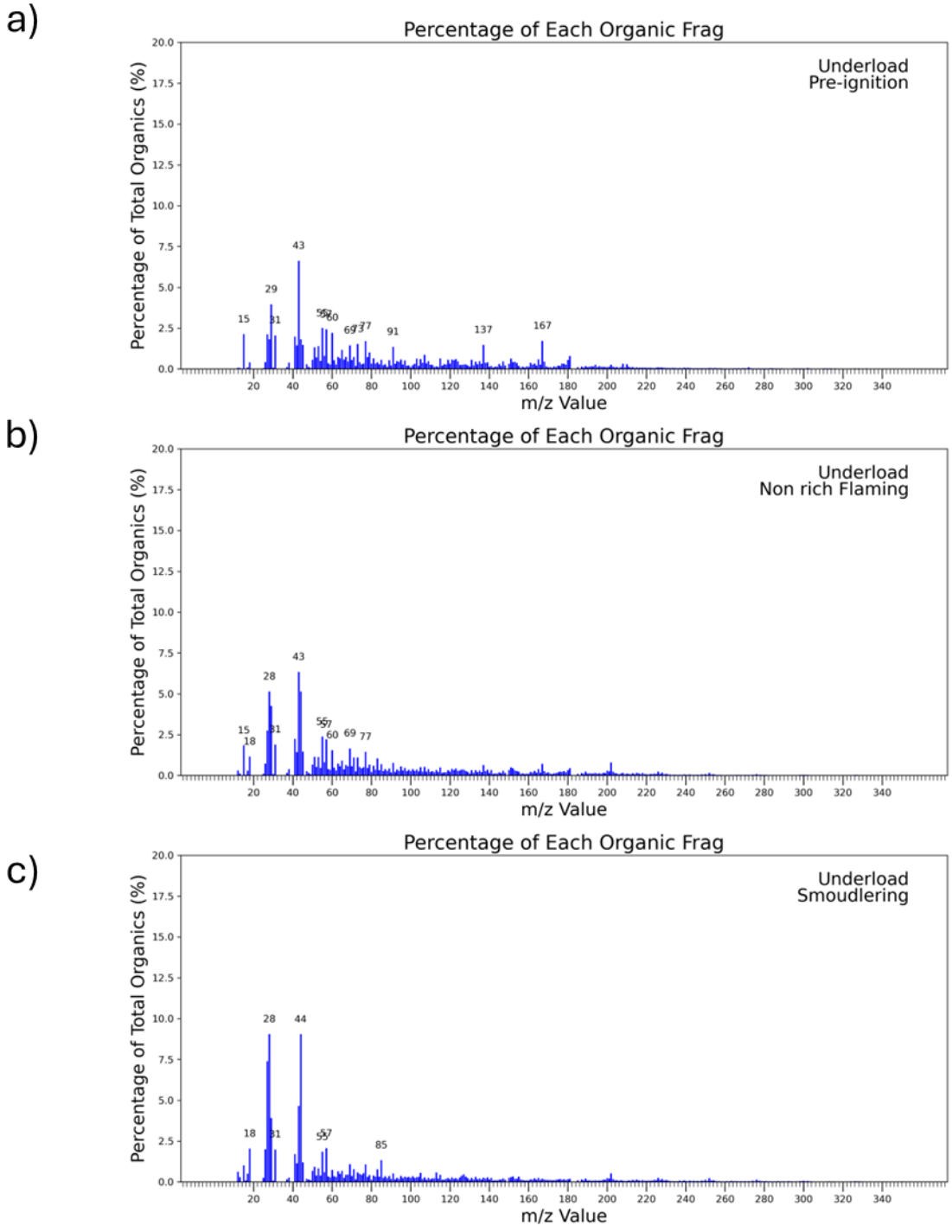

Figure S9 Mass spectra from AMS for Underload protocols by phases.

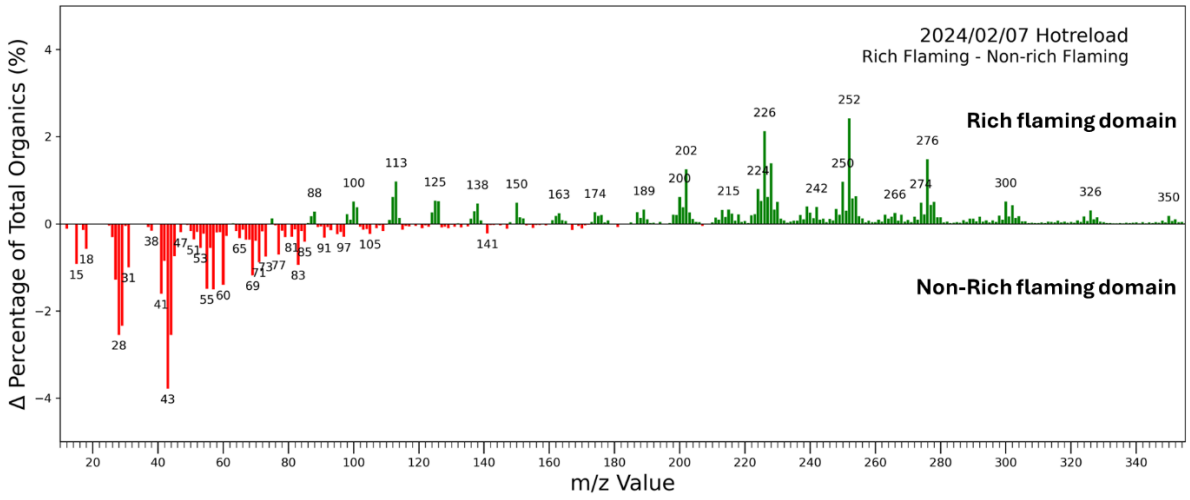

Figure S10 Difference of organic aerosols averaged mass spectra for rich flaming from base case (non-rich flaming) for hot reload protocol.

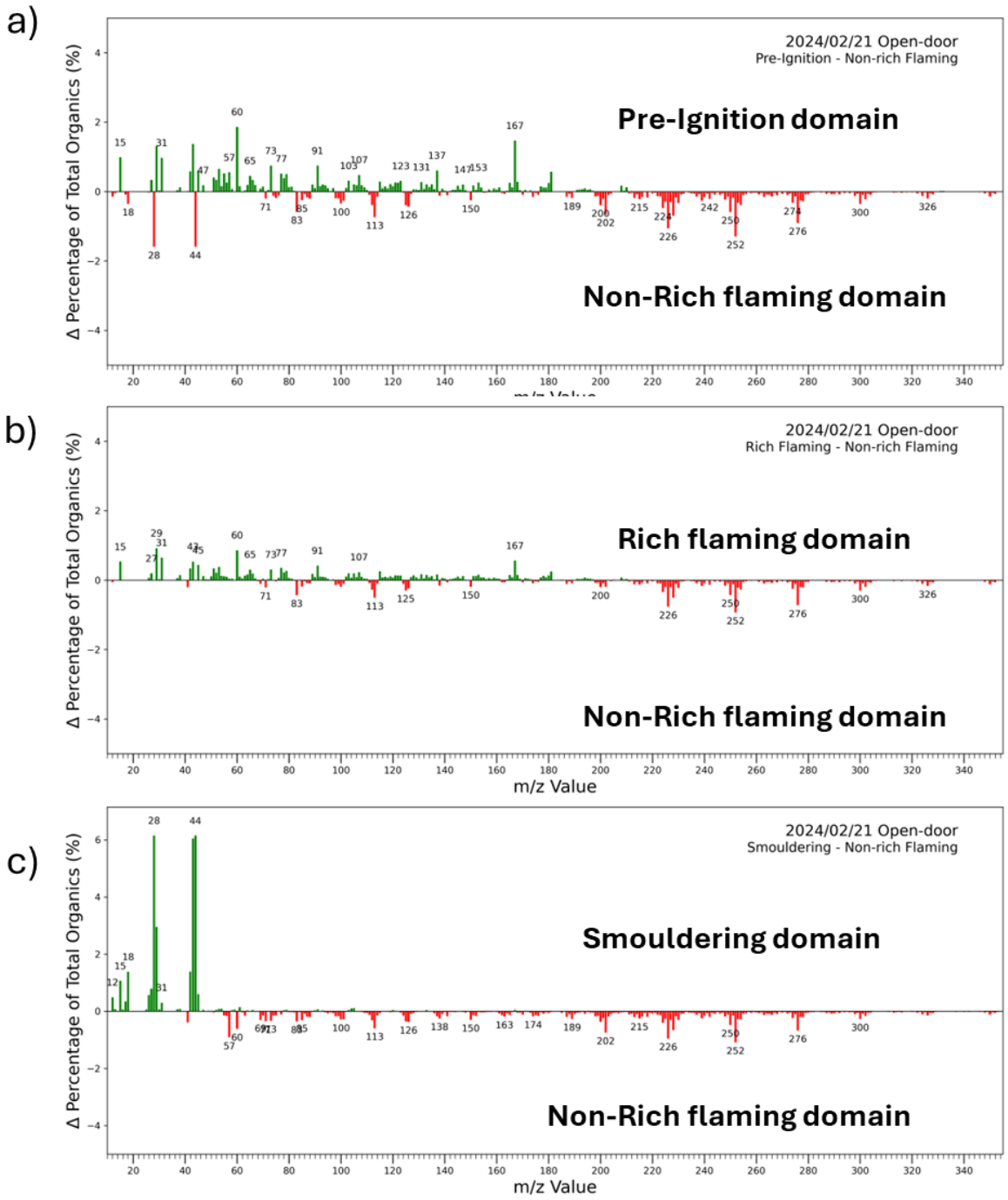

Figure S11 Difference of organic aerosols averaged mass spectra for a) pre-ignition and b) rich flaming and c) smouldering from base case (non-rich flaming) for open-door protocol.

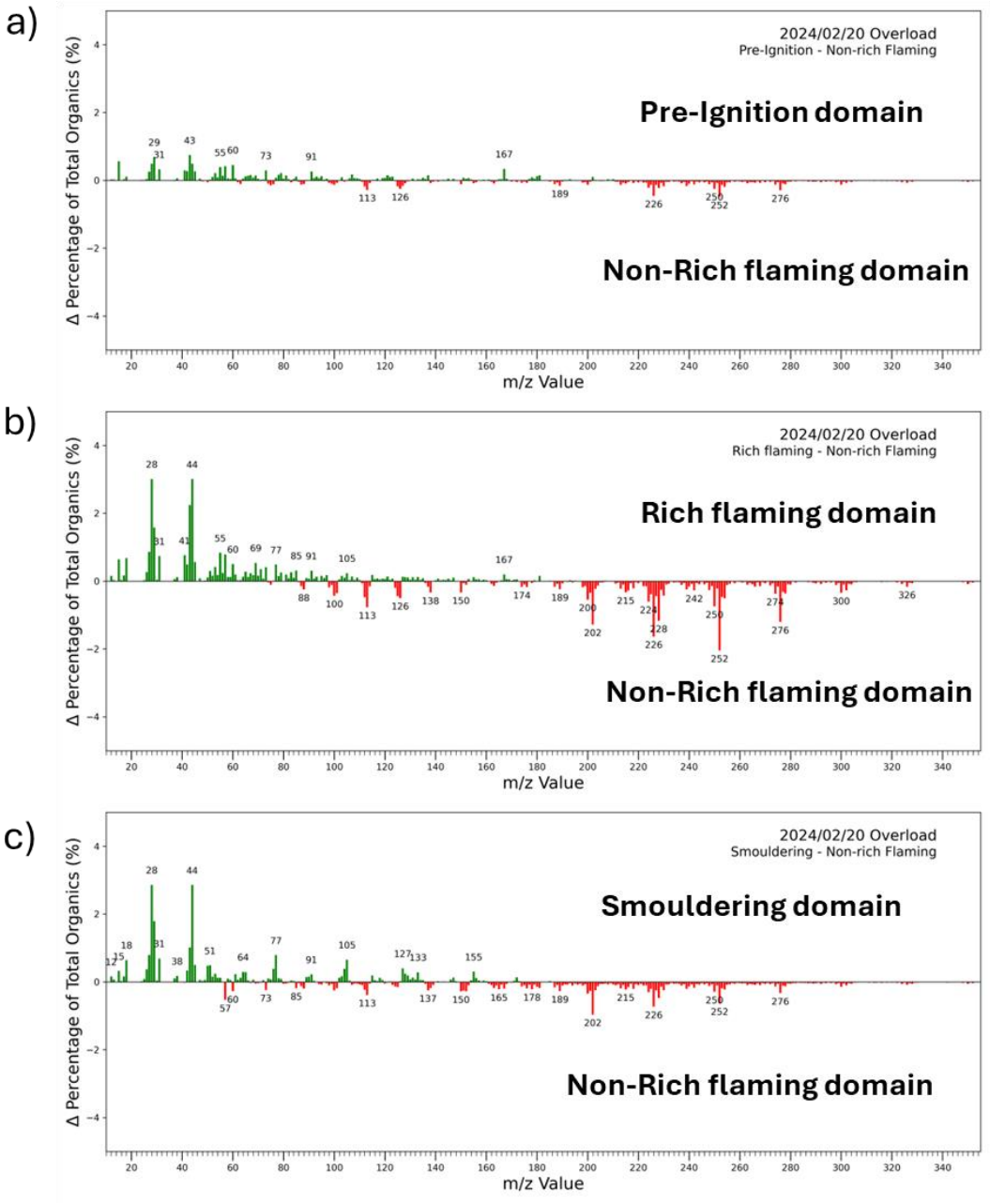

Figure S12 Difference of organic aerosols averaged mass spectra for a) pre-ignition and b) rich flaming and c) smouldering from base case (non-rich flaming) for overload protocol.

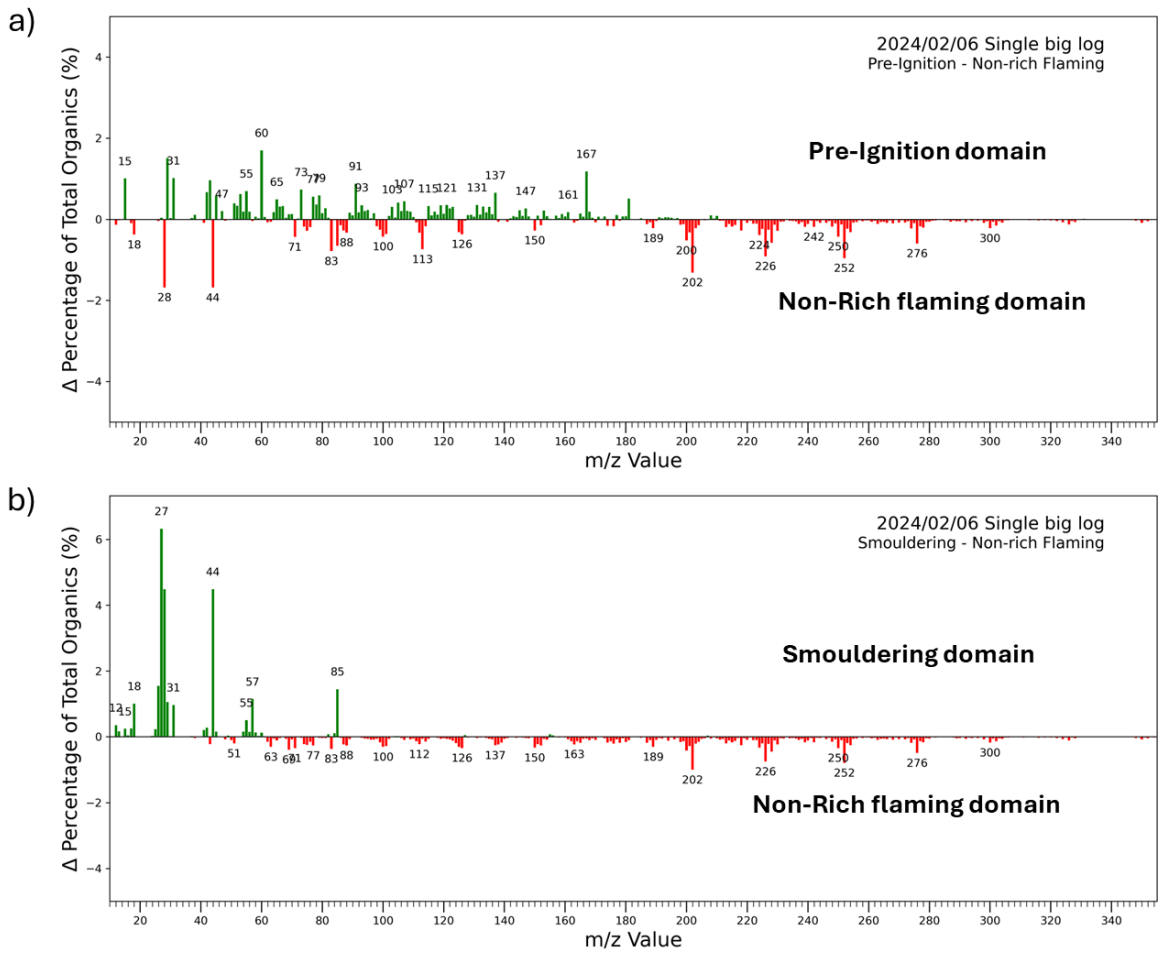

Figure S13 Difference of organic aerosols averaged mass spectra for a) pre-ignition and b) smouldering from base case (non-rich flaming) for single big log protocol.

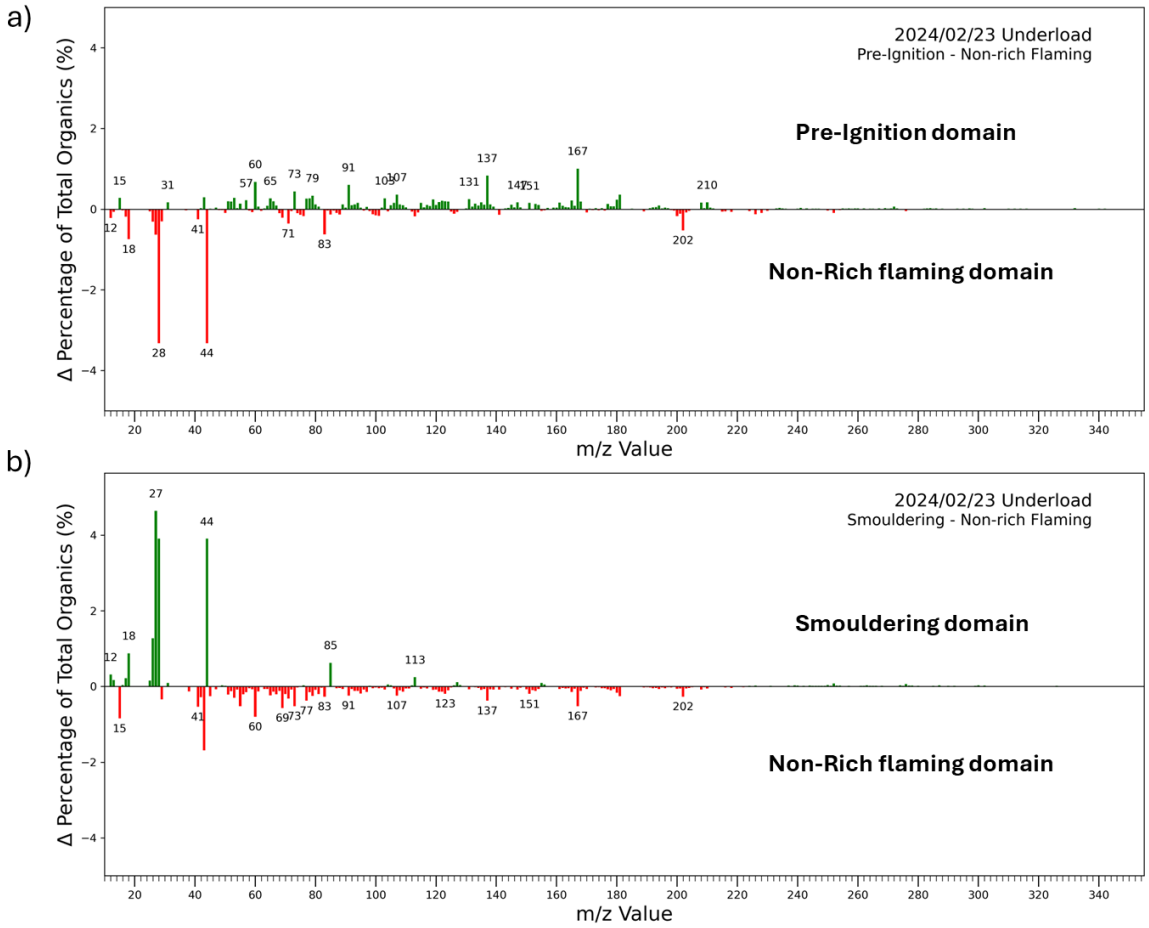

Figure S14 Difference of organic aerosols averaged mass spectra for a) pre-ignition and b) smouldering from base case (non-rich flaming) for underload protocol.

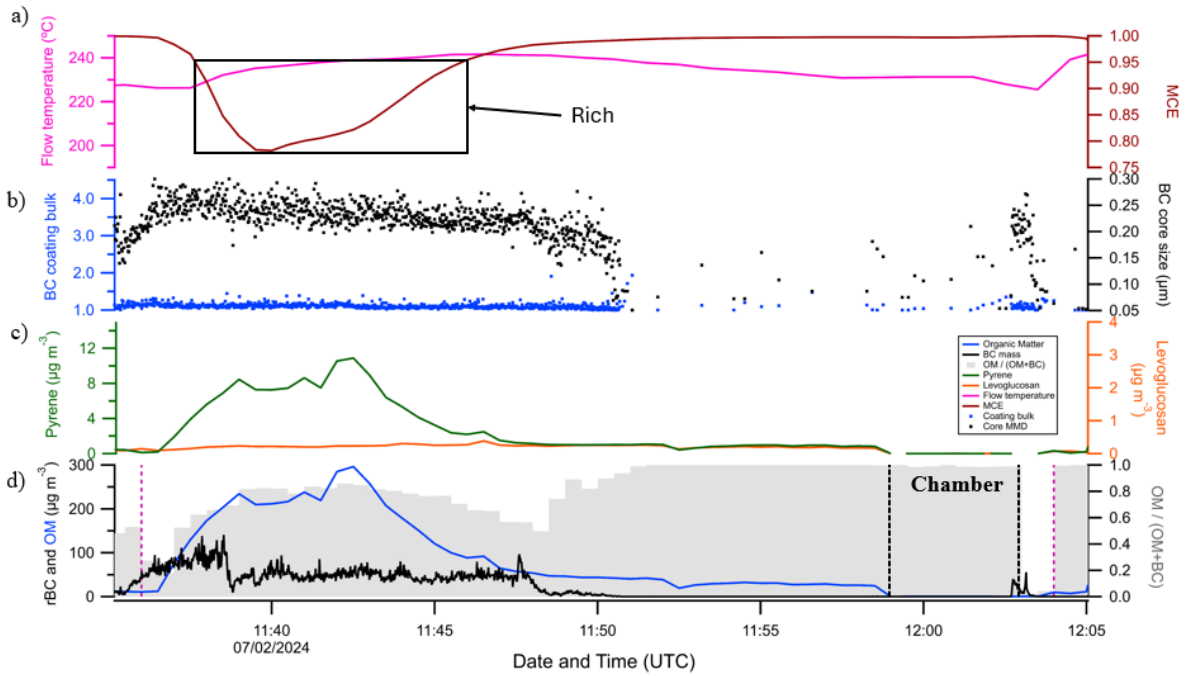

Figure S15 Time series of a hot reload burn cycle. Rich flaming periods are annotated. Under the standard burn protocol, both rBC and OM remained elevated, while the OM/(OM+BC) ratio decreased sharply. However, deviations were evident in other operations such as hot reload in this figure, where OM emissions were substantially higher, likely due to incomplete oxidation of pyrolysis products.

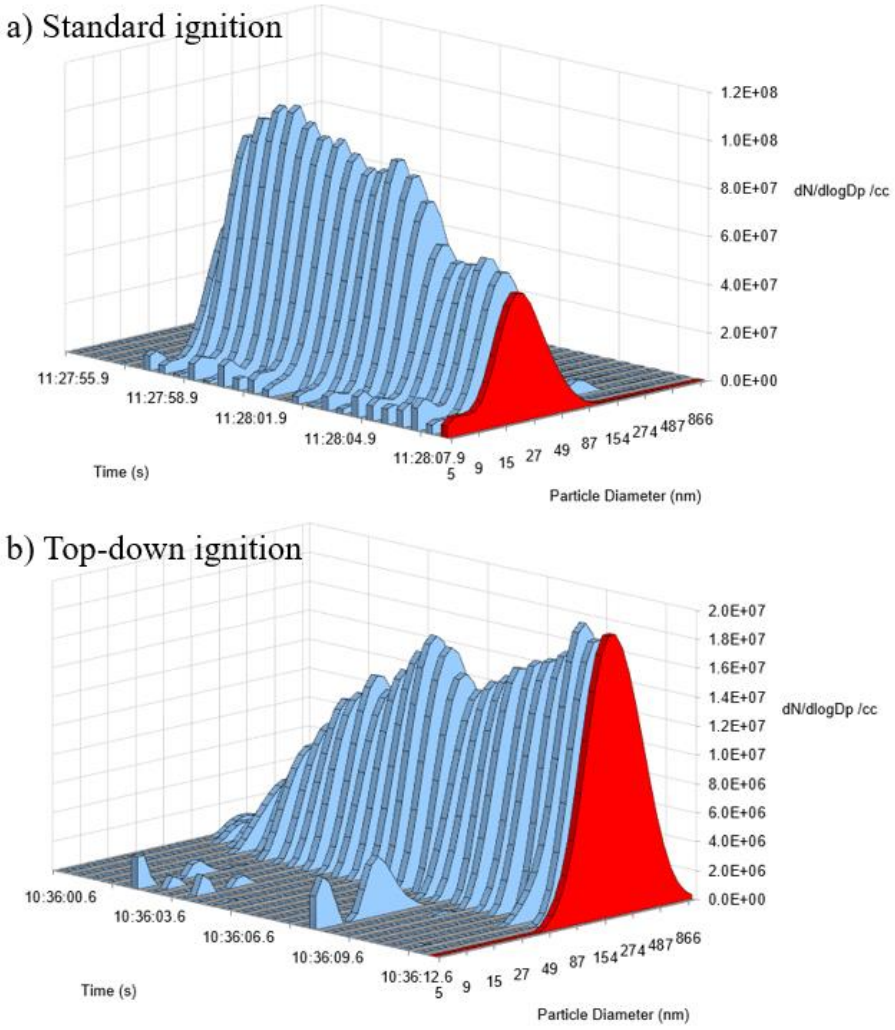

Figure S16 DMS500 size distribution time series for the first 12 seconds of ignition for a) a standard burn cycle and b) the top-down ignition test burn cycle.

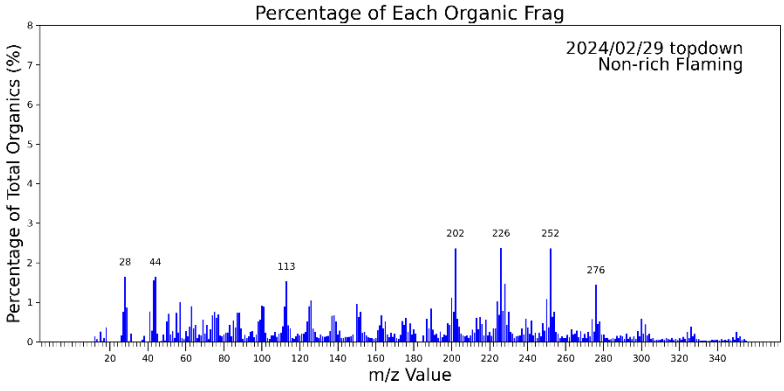

Figure S17 Mass spectra from AMS for top-down ignition test burn cycle.

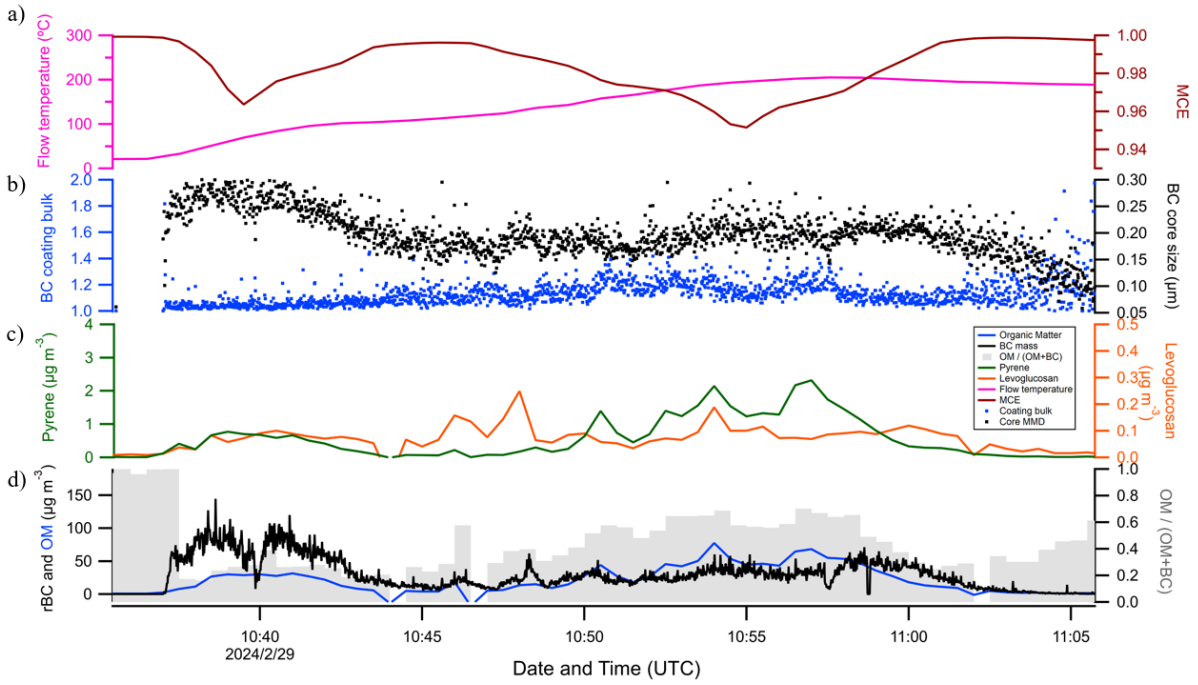

Figure S18 Time series of the top-down ignition burn cycle.